


CONTACT ANGLE ESTIMATION THROUGH GAUSSIAN SMOOTHING QUANTIFICATION

ESTIMAÇÃO DO ÂNGULO DE CONTATO ATRAVÉS DA QUANTIFICAÇÃO DA SUAVIZAÇÃO GAUSSIANA

ESTIMACIÓN DEL ÁNGULO DE CONTACTO MEDIANTE CUANTIFICACIÓN DE SUAVIZADO GAUSSIANO

 <https://doi.org/10.56238/edimpecto2025.034-008>

Antonio Henrique Figueira Louro¹, Swami de Paula Lima², Jauberth Weyll Abijaude³

ABSTRACT

This paper presents a new method for measuring the contact angle of sessile droplets. The method is based on Gaussian smoothing of a binary image of a droplet, followed by subtraction of its binary version. This result quantifies the smoothing produced at each pixel. Due to the circular symmetry of the 2D Gaussian, it is possible to establish a direct relationship between the smoothing produced at the pixel and the angular configuration of its surroundings. The method is quite accurate and, in the case of images with good contrast, the procedure can be fully automated, requiring only that the operator indicate the contact line between the droplet and the solid surface.

Keywords: Sessile Drop. Contact Angle. Gaussian Difference.

RESUMO

Este artigo apresenta um novo método para medir o ângulo de contato de gotas sésseis. O método é baseado na suavização gaussiana da imagem binária de uma gota, com a subsequente subtração de sua versão binária. Este resultado quantifica a suavização produzida em cada pixel. Devido à simetria circular da gaussiana 2D é possível estabelecer uma relação direta entre a suavização produzida no pixel e a configuração angular de sua vizinhança. O método é bastante preciso e, no caso de imagens com bom contraste, o procedimento pode ser totalmente automático, exigindo apenas que o operador indique a linha de contato entre a gota e a superfície sólida.

Palavras-chave: Gota Sésseil. Ângulo de Contato. Diferença de Gaussianas.

RESUMEN

Este artículo presenta un nuevo método para medir el ángulo de contacto de gotitas sésiles. El método se basa en el suavizado gaussiano de una imagen binaria de una gotita, seguido de la sustracción de su versión binaria. Este resultado cuantifica el suavizado producido en cada píxel. Debido a la simetría circular de la gaussiana 2D, es posible establecer una relación directa entre el suavizado producido en el píxel y la configuración angular de su entorno. El método es bastante preciso y, en el caso de imágenes con buen contraste, el

¹ Dr. in electrical engineering. Universidade Estadual de Santa Cruz. E-mail: louro@uesc.br

² Bachelor's degree: computer science. Universidade Estadual de Santa Cruz. E-mail: splima.cic@uesc.br

³ Doctorate student in computer science. Universidade Estadual de Santa Cruz. E-mail: jauberth@uesc.br



procedimiento puede automatizarse completamente, requiriendo únicamente que el operador indique la línea de contacto entre la gotita y la superficie sólida.

Palabras clave: Gota Sésil. Ángulo de Contacto. Diferencia Gaussiana.

1 INTRODUCTION

Surface science involves studies of properties and characteristics of solid surfaces and their interactions with liquids. The fundamental understanding of these interactions such as wetting, spreading, adhesion and dehumidification, is not only crucial for science itself, but also of great value for a large number of distinct industrial applications.

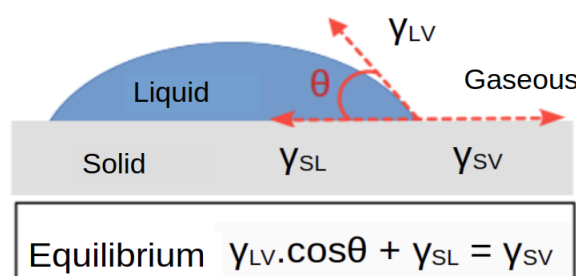
Contact angle measurement is a way to assess whether a surface has hydrophobic or hydrophilic characteristics. It is based on the observation of the intermolecular interactions between a small droplet of water (or other liquids) and the surface on which it is deposited. The measurement of the contact angle is easily conducted by establishing the tangent angle to the droplet region where the intersection of the three phases (solid, liquid and gas) occurs.

The contact angle is defined as the mechanical equilibrium of the droplet under the action of three interfacial stresses: solid-vapor (γ_{sv}); solid-liquid (γ_{sl}) and liquid-vapor (γ_{lv}). This equilibrium relationship is known as Young's equation (Law, Zhao, 2015). Fig. 1 shows a diagram showing this equilibrium condition and the contact angle on the right side of the droplet profile.

The liquid droplets are usually in the millimeter range. The smaller the droplet, the greater the effect of the surface tension of the liquid. The most widely used technique for measuring contact angles is the sessile drop method, a static drop on a surface. Low contact angle values demonstrate a tendency of water to spread and adhere to the surface, while high contact angle values show the tendency of the surface to repel water.

Figure 1

Contact angle



Source: The Author (2023).

Older measurements, such as Young's, used a protractor to measure the angle. Several other techniques were developed based on the assumption that the sessile drop is spherical, or part of a sphere, so the contact angle values were calculated using principles of

Euclidean geometry. The complexity of contact angle analysis can range from simple visual estimates, using some angle measurement tool, to mathematically rigorous techniques such as the class of methods known as axisymmetric drop shape analysis (ADSA), based on the numerical adjustment between the drop shape and the mathematical model given by the Young-Laplace capillarity equation (William *et al.*, 2010).

This work presents an angular estimation technique distinct from any other existing one, which is based on the quantification of the brightness received (or given) in each pixel of a binary image as a result of Gaussian smoothing. The objective is to show the ability of the method to estimate angles. Therefore, techniques involving image enhancement, detection of straight lines (Hough transform) and active contours (snakes), which can be of great value in making the method completely automatic, are left for future work. For now, the only concern regarding the appearance of the input image is to ensure that the object of interest has dimensions at least twice as large as the largest convolution window used.

2 THE PROPOSED METHOD

The method presented here derives from the work developed in Louro (2016) used to detect *Corners* in contours and determine those that really have an influence on the shape of the object, which are the vertices of its convexities and concavities. Its operation is fundamentally a Gaussian difference (DoG) operation in binary images, operating at multiple scales.

In the case of applying the method to images of sessile drops, the multiscale scheme is simpler, since it is already known in advance that there are only two vertices in its profile, which are the vertices of the contact angles. In addition, the shape of a drop is quite soft. Thus, the proposed method uses two scales. A very low scale ($\sigma=0.5$) with the aim of precisely locating all candidates for *corner* and a very high scale ($\sigma=23,833$) to keep only the *Corners* that matter.

Although the fundamental idea is simple, there are many details that need to be highlighted before describing how the method works. Such details involve Gaussian smoothing of binary images, basic concepts of scaling and how it is possible to have a relationship between smoothing and angular values.

2.1 BASIC THEORY

The two-dimensional Gaussian function (2D), presented in Eq. (1), is used in image processing and analysis to filter or smooth images, as well as to produce multiscale representations. The standard deviation (σ) is the parameter used to determine the Gaussian aperture. The higher its value, the higher the scale, the greater the intensity of the smoothing and the lower the frequencies admitted by the filter.

$$f(x, y) = \frac{1}{2\pi\sigma^2} e^{-[(x-\mu_x)^2 + (y-\mu_y)^2]/(2\sigma^2)} \quad (1)$$

The 2D Gaussian is shaped like a bell, but digitally it is implemented in a square window with coefficients arranged in a circularly symmetrical manner, with the values decaying from the center toward the periphery. In its continuous representation, the Gaussian tail extends to infinity. However, when considering Gaussian as a statistical distribution, the rule of thumb says that between -3σ and $+3\sigma$ there is a 99.7% probability of finding the desired data (Ozdemir, 2016). Thus, windows where Gaussian is digitally implemented usually have a width corresponding to 6σ . For example, a Gaussian with $\sigma=0.5$ is usually snapped to a 3×3 window.

Gaussian smoothing promotes the transfer of brightness from white pixels to black pixels. The importance of this information lies in the choice of the direction of the subtraction operation used in the quantification of smoothing. If the object of interest is white on a black background, the operation will be "*binary image minus smoothed image*". This operation reports the amount of brightness given by the object's pixels. In the opposite case, where you want to detect characteristics of a black object on a white background, the operation should be "*smoothed image minus binary image*", which quantifies the brightness received by the object's pixels (Louro, 2016).

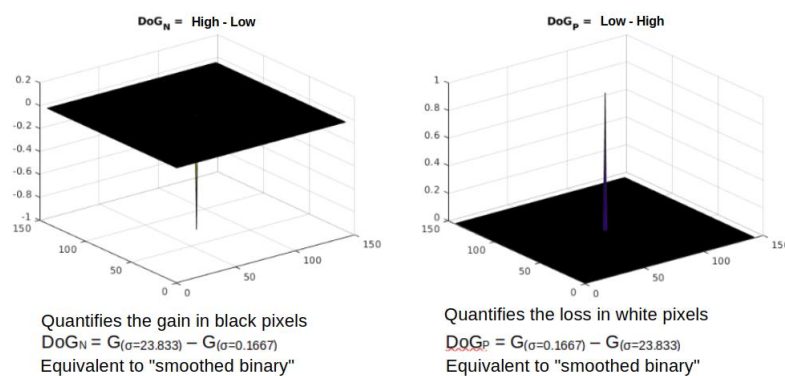
At the beginning of this section, it was stated that the method is fundamentally a Gaussian difference operation. However, only one of the subtraction plots is a smoothed image. The other is a binary image with no smoothing at all. This leads one to believe that the statement is not correct. However, it is possible to consider the binary image as having undergone smoothing with a very small nucleus, confined to a region smaller than a pixel, that is, $6\sigma \leq 1$. Such smoothing does not cause any modification in the binary image. Therefore, it is okay to consider the proposed method to be a Gaussian difference. To

differentiate this operation from DoG, from this point on, the proposed method will be referred to as DoGz, mentioning that one of the subtraction plots has been smoothed with a Gaussian whose $\sigma \rightarrow 0$. Figure 2 shows the DoGz nuclei whose convolutions with the binary image produce the same result as the subtraction between the binary and smoothed images.

The square window containing the implementation of a Gaussian can be thought of as a circle, since its coefficients are arranged in a circularly symmetrical fashion. So, one can imagine that the local neighborhood comprised by the window also has a circular shape. It is exactly this circular shape that gives rise to the relationship between the result DoGz and angular values.

Figure 2

Result of the subtraction of two Gaussians. One with $\sigma=0.1667$ and the other with $\sigma=23.833$



Source: The Author (2023).

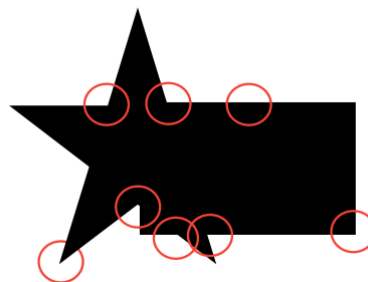
Figure 3 exemplifies some moments of the convolution, where the Gaussian nucleus, represented by a red circle, is centered on the contour of the object. It should be noted that the content of these neighborhoods is composed of object and background regions, which produce complementary circular sectors. These vary according to the local shape of the object, that is, whether it is a protrusion of the object advancing over the background, whether it is an indentation of the object, where the background advances over the object, or whether it is a straight edge.

The DoGz response, for a pixel situated on the object's outline, represents the angle of the circular sector that is formed in the input neighborhood. This response becomes stronger as the industry angle narrows. This is explained by the fact that there is a smaller

number of pixels of the object and a greater number of background pixels within the neighborhood. The greater this difference, the greater the amount of brightness transferred between this pixel and the background pixels during the smoothing process (Louro, 2016).

Figure 3

Gaussian nucleus (red circle) forming circular sectors along the object-ground boundary



Source: The Author (2023).

Another way to refer to the Gaussian aperture is to use the term scale, which brings the idea of observation distance. Observing a scene on a low scale means observing it from a short distance, restricting the acquisition of information to a small region of the scene at a time, losing track of the whole. On the other hand, it allows you to observe and locate details more easily. This is exactly what happens when using a small (σ small) convolution window.

In the case of a binary image, its low-scale smoothing causes modifications only in the boundary between the object and the background. Consequently, the resulting DoGz image exhibits intensities perceptible only along the outline of the object, whose values reflect the local shape of the boundary such as convexities, concavities, straight-line edge, scan noises, and unimportant details. To confirm whether these characteristics have an influence on the overall shape of the object, it is necessary to verify whether their importance is maintained on higher scales.

To estimate the convexity angles and concavities of objects, small-scale observation presents two problems. The first is that in small windows (3x3), centered on the contour, the number of possible configurations of the object-background is quite limited, reflecting the limited number of circular sectors that can be produced. That is, they have low angular resolution. Figure 4 shows the eight possible configurations centered on the outline. These can appear rotated relative to the central pixel. Each of them produces its own DoGz response, which is shown in Table 1.



The second problem can be seen with the help of Fig. 4 and Table 1. The 90° setting, for example, has two distinct DoGz values. These depend on whether the angle is formed by diagonal edges or by horizontal and vertical edges. The serrated effect that appears in the representation of slanted edges, known as *aliasing*, is responsible for producing distinct DoGz responses to the same angle. With the increase in scale, both problems are mitigated. On the one hand, angular resolution grows and on the other, the effect of *aliasing* Decreases.

The values of the contact angles of sessile droplets can vary greatly with the type of liquid and surface used, requiring the method to be able to represent the largest possible number of angles. Thus, it was decided to estimate the angles on the highest scale used by the method ($\sigma=23.833$).

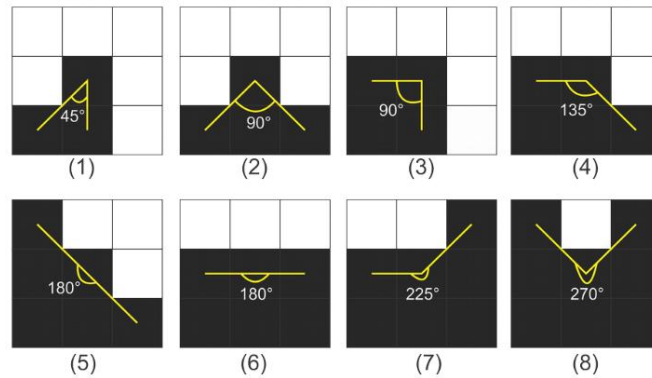
To produce the "DoGz response - angle" relationship at the highest scale, configurations similar to those in Fig. 4 were constructed and some more with smaller angles. However, all with a size proportional to that of the 143x143 window. Next, the DoGz was computed in each of these configurations and the resulting values were used in a linear interpolation process, which produced values corresponding to all integer angles between 0° and 360°, which were stored in an angle table.

2.2 HOW THE DOGZ METHOD WORKS

The entire following explanation is based on the case of a black object on a white background. The input image must be grayscale and cropped exactly over the contact line, discarding the bottom portion. The resulting image is converted into binary with the aid of Otsu's automatic threshold (Otsu, 1979). Before smoothing, the process of *Padding* of at least 72 pixels.

Figure 4

The eight possible angular contour configurations in a 3x3 window



Source: The Author (2023).

Table 1

Some angular configurations and their respective DoGz responses

Angle	DoGz output by scale (σ)	
	$\sigma = 0.5$ (3x3 window)	$\sigma = 23.8333$ (143x143 window)
45th	0.2855	0.8677
90o (diagonal)	0.2741	0.7440
90o(H/V)	0.2017	0.7415
135th	0.1903	0.6178
180o (diagonal)	0.1790	0.4940
180o (H or V)	0.1065	0.4916
225th	0.0952	0.3679
270th	0.0838	0.2441

Source: The Author (2023).

Two Gaussian smoothings are made. The first with $\sigma = 0.5$ and the other with $\sigma = 23.8333$. After each smoothing, the binary version is subtracted from the smoothed version, producing the DoGz image. From the first DoGz image, all pixels with a value greater than 0.179 and less than 0.2855 are selected (see Table 1). Its coordinates and values are copied to a table of convexity vertex candidates. With the aid of the second DoGz image, this table is complemented with the values presented by the same candidates on a large scale. Next, a descending order is made in the table with respect to the high-scale DoGz values, providing the coordinates and DoGz values of the vertices of the two contact angles. The values of these vertices are converted into angles by accessing the angle table and classifying them by minimum distance. Figure 5 shows the flowchart of the proposed method,

which is valid for good quality images, whose binarization is simple. In the next section, another simpler algorithm is presented, but it is dependent on the experience of the operator.

3 RESULTS AND DISCUSSIONS

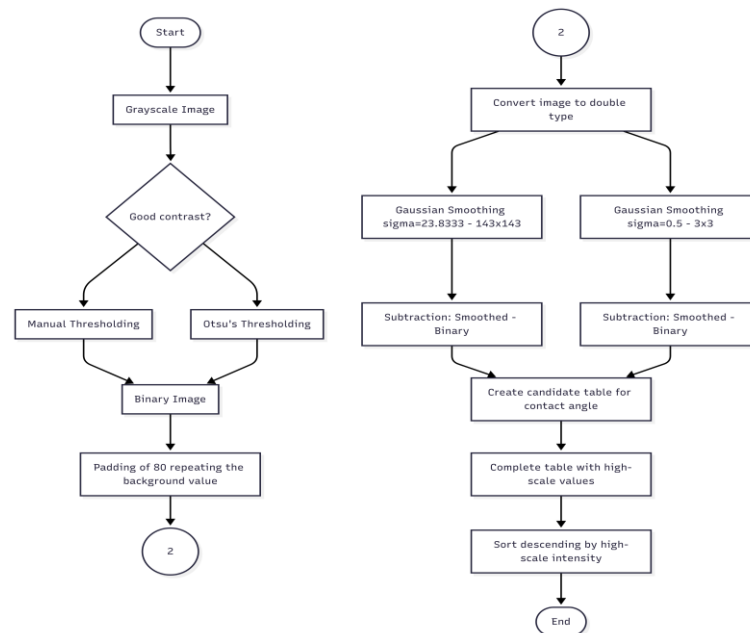
The software and tests were developed at Matlab. The images used in the tests have two origins: scientific articles and the camera of a Samsung Galaxy A01 smartphone coupled to an Apexel 12.5X macro lens. As backlight, a 24W LED ceiling light with cold white light was used. The entrance images have not undergone any improvement. However, some had to have their dimensions doubled, or quadrupled. This was done for two distinct reasons. The first, to make the object of interest larger than the 143x143 convolution window. The second, to prevent defects in the binary image from interfering with the convolution window when it is centered at the vertices of the contact angles. Figure 6 shows the reason for this enlargement of the image. A similar solution would be to work with the Gaussian core on a smaller scale, however smaller scales imply lower angular resolution and greater influence of the *aliasing*.

The images of sessile drops available in many scientific articles usually present a very accentuated specular reflex, similar to what is shown in Fig. 6. This undesirable characteristic prevents the use of the algorithm described in Fig. 5, mainly because it presents more than two candidates for real vertices. For example, in Fig. 6, the binary image has four vertices. Two are the vertices of the contact angles and two are the internal vertices at the base of the hole generated by the specular reflection.

For images that present an unsuccessful binarization, such as the one in Fig. 6, DoGz is applied only at the highest scale. There is no analysis of vertex candidates. These are defined as the two extreme pixels (right and left) of the base of the droplet. Then, just check the values of these pixels in the DoGz image and access the angle table to get the respective angles.

Figure 5

Flowchart of the proposed method



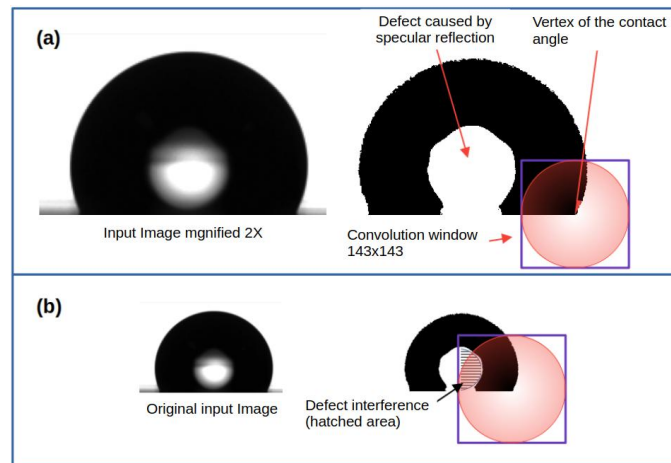
Source: The Author (2023).

3.1 TESTS ON IMAGES AVAILABLE IN SCIENTIFIC ARTICLES

Table 2 shows the comparison between the results of five published studies and the response of the proposed DoGz method. One of the studies does not report how the contact angles were measured. The others used automatic goniometers with their respective proprietary software.

Figure 6

Image enlargement to avoid the defects caused by binarization. (a) the scale-up allows the scale adopted to achieve "clean" circular sectors. (b) the scale adopted is greater than the width of the object, introducing "background pixels in the circular sector"



Source: The Author (2023).

3.2 TESTS ON IMAGES AVAILABLE IN SCIENTIFIC ARTICLES

Table 2 shows the comparison between the results of five published studies and the response of the proposed DoGz method. One of the studies does not report how the contact angles were measured. The others used automatic goniometers with their respective proprietary software.

Most of the comparisons showed very close results. However, some were quite discrepant, for example the result of Brown and Bhushan (2016) in their figure 3b, which differs from DoGz by 24°. The main reason is the uncertainty in the location of the line of contact between the droplet and the surface. The closest DoGz response (not shown) to this image was 154°, using various techniques to enhance the image. Figure 7 shows that visually it is difficult to reach the 163o informed by the author.

Table 2

Comparison between published results and the DoGz response.

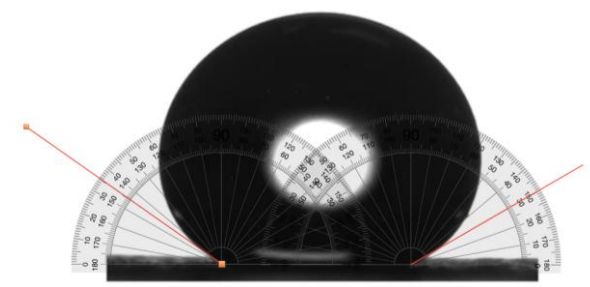
Work/Method	Image reference	Work Results	DoGz Results
(Kerstner <i>et al.</i> , 2014)	Figure 3a	63o +/- 1.4o	Right = 63o, Left = 61o
	Figure 3b	105o +/- 1.7o	Right = 104°, Left = 105°
Method not informed	Figure 3c	116o +/- 1.9o	Right = 113°, Left = 110°

	Figure 3d	114o +/- 1.0o	Right = 107°, Left = 112°
	Figure 3e	86o +/- 0.8o	Right = 77°, Left = 78°
(Tong <i>et al.</i> , 2019) - Ramé-	Figure 9a	71.7th	Right = 61°, Left = 62°
Hart automated goniometer	Figure 9b	111.7th	Right = 107°, Left = 101°
	Figure 9c	34.30o	Right = 37°, Left = 37°
	Figure 9d	75.65th	Right = 68°, Left = 62°
(Brown, Bhushan, 2016) -	Figure 3a (column 1)	76th +/- 1st	Right = 74°, Left = 70°
automated goniometer	Figure 3b (column 1)	163rd +/- 2nd	Right = 139°, Left = 139°
(Model 290, Ramé -Hart	Figure 3c (Column 1)	165o +/- 2o	Right = 137°, Left = 138°
Inc/ DroplImage software	Figure 3d (column 2)	12th +/- 2nd	Right = 15th, Left = 17th
	Figure 3e (column 2)	100° +/- 2°	Right = 93°, Left = 96°
	Figure 3f (column 2)	154th +/- 2nd	Right = 152o, Left = 153o
(Liu <i>et al.</i> , 2016)	Figure 4a	81st	Right = 77°, Left = 81°
optical contact angle meter	Figure 4b	36th	Right = 29°, Left = 36°
OCA20	Figure 4c	82nd	Right = 81°, Left = 80°
	Figure 4d	52nd	Right = 45°, Left = 49°
(Guisbiers <i>et al.</i> , 2012) -	Figure 2a	47.2o +/- 1.9o	Right = 42°, Left = 44°
Contact Angle Meter GBX	Figure 2b	74.4o +/- 1.8o	Right = 75°, Left = 73°
	Figure 2c	83.6o +/- 4.2o	Right = 85°, Left = 89°
	Figure 2d	102.2o +/- 5.5o	Right = 111°, Left = 105°

Source: The Author (2023).

Figure 7

Measurement, with protractor, of figure 3b contained in (Brown, Bhushan, 2016)



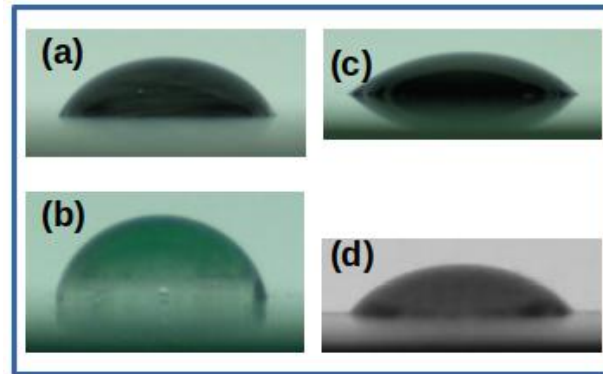
Source: The Author (2023).

3.3 SMARTPHONE IMAGE TESTS

This test is applied to the images shown in Fig. 8 and the DoGz responses are compared to the responses of three methods made available as plugins of the ImageJ software. They are: Low-Bond Axi-symmetric Drop Shape Analysis (LBADSA) (Stalder *et al.*, 2010); Contact Angle Analysis routine (Brugnara, 2006) and DropSnake (Stalder *et al.*, 2006).

Figure 8

Images obtained with a smartphone



Source: The Author (2023).

4 CONCLUSIONS

In this work, an unprecedented method for computing angles in binary images is proposed, which is applied to estimate contact angles in sessile droplet profiles. It uses a very simple and widely known technique in the field of computer vision, which is the Gaussian difference (DoG). The results presented are quite promising. However, it is necessary to improve the method to make it fully automatic and robust to lighting problems.

Table 3

Comparison between ImageJ and DoGz plugins for the images in Figure 8

Image	Contact Angle	DropSnake	LBADSA	DoGz
Figure 8a	D=68.7o, E=66.3o	D=63.9o, E=58.1o	58.8o	D=66o, E=67o
Figure 8b	D=77.6o, E=79.7o	D=78.2o, E=74.3o	81.18th	D=73o, E=75o
Figure 8c	D=45.1o, E=38.9o	D=36.3o, E=32.9o	41.5o	D=38o, E=35o
Figure 8d	D=55o, E=56.4o	D=39.5o, E=42.9o	47.5th	D=43o, E=45o

Source: The Author (2023).

ACKNOWLEDGEMENTS

This research is funded by the State University of Santa Cruz – Law 8.352/2002 CONSEPE 64/2019 – Ordinance 573/2021 – 12/15/2021.

REFERENCES

- Brown, P. S., & Bhushan, B. (2016). Durable, superoleophobic polymer–nanoparticle composite surfaces with re-entrant geometry via solvent-induced phase transformation. *Scientific Reports*, 6(1), 1–11. <https://doi.org/10.1038/srep21048>
- Brugnara, M. (2006). Contact angle plugin for ImageJ software. Trento, IT.
- Guisbiers, G., Arscott, S., & Snyders, R. (2012). An accurate determination of the surface energy of solid selenium. *Applied Physics Letters*, 101(23). <https://doi.org/10.1063/1.4769893>
- Kerstner, E. K., Kunst, S. R., Beltrami, L. V. R., Vega, M. R. O., Scienza, L. C., & Malfatti, C. de F. (2014). Anticorrosive performance of commercial nanoceramic coatings on AISI 1010 steel. *Materials Research*, 17(6), 1497–1506. <https://doi.org/10.1590/1516-1439.292814>
- Law, K. Y., & Zhao, H. (2015). *Surface wetting: Characterization, contact angle, and fundamentals* (1st ed.). Springer International Publishing.
- Liu, H., Ma, J., Zhu, C., Xu, J., & Gong, J. (2016). Miscibility and crystallization behavior of poly(ethylene terephthalate)/phosphate glass hybrids. *Journal of Applied Polymer Science*, 55(11), 1039–1050. <https://doi.org/10.1002/app.44048>
- Louro, A. H. F. (2016). A suavização gaussiana como método de marcação de características de fronteira entre regiões homogêneas contrastantes [Doctoral dissertation, Escola de Engenharia de São Carlos]. <https://doi.org/10.11606/T.18.2016.tde-29072016-164415>
- Otsu, N. (1979). Threshold selection method from gray-level histograms. *IEEE Transactions on Systems, Man, and Cybernetics*, SMC-9(1), 62–66. <https://doi.org/10.1109/TSMC.1979.4310076>
- Ozdemir, S. (2016). *Principles of data science: Learn the techniques and math you need to start making sense of your data* (1st ed.). Birmingham, UK: Packt Publishing.
- Stalder, A. F., Kulik, G., Sage, D., Barbieri, L., & Hoffmann, P. (2006). A snake-based approach to accurate determination of both contact points and contact angles. *Colloids and Surfaces A: Physicochemical and Engineering Aspects*, 286(1–3), 92–103. <https://doi.org/10.1016/j.colsurfa.2006.03.008>
- Stalder, A. F., Melchior, T., Müller, M., Sage, D., Blu, T., & Unser, M. (2010). Low-bond axisymmetric drop shape analysis for surface tension and contact angle measurements of sessile drops. *Colloids and Surfaces A: Physicochemical and Engineering Aspects*, 364(1–3), 72–81. <https://doi.org/10.1016/j.colsurfa.2010.04.030>
- Tong, C., McCarthy, S., Li, Z., Guo, J., Li, Q., Pacheco, C. N., & others. (2019). Hybrid polyphosphazene-organosilicon polymers as useful elastomers. *ACS Applied Polymer Materials*, 1(7), 1881–1886. <https://doi.org/10.1021/acsapm.9b00410>



Williams, D., Kuhn, A., Amann, M., Hausinger, M., Konarik, M., & Nesseirod, E. (2010, October). Computerised measurement of contact angles. *Galvanotechnik*, 1–10.